



HAL
open science

Introducing a moving load in a simulation in time over a truncated unbounded domain

Patryk Dec, Régis Cottureau, Baldrik Faure

► To cite this version:

Patryk Dec, Régis Cottureau, Baldrik Faure. Introducing a moving load in a simulation in time over a truncated unbounded domain. 2022. hal-03681082v1

HAL Id: hal-03681082

<https://hal.science/hal-03681082v1>

Preprint submitted on 30 May 2022 (v1), last revised 10 Oct 2023 (v2)

HAL is a multi-disciplinary open access archive for the deposit and dissemination of scientific research documents, whether they are published or not. The documents may come from teaching and research institutions in France or abroad, or from public or private research centers.

L'archive ouverte pluridisciplinaire **HAL**, est destinée au dépôt et à la diffusion de documents scientifiques de niveau recherche, publiés ou non, émanant des établissements d'enseignement et de recherche français ou étrangers, des laboratoires publics ou privés.

Introducing a moving load in a simulation in time over a truncated unbounded domain

Patryk Dec^{a,b}, Régis Cottereau^{a,*}, Baldrik Faure^b

^a*Aix-Marseille Univ., CNRS, Centrale Marseille, LMA
4 impasse Nikola Tesla, 13013 Marseille, France*

^b*SNCF, Innovation and Research Department,
1/3 avenue François Mitterrand, 93212 La Plaine Saint Denis, France*

Abstract

When using Finite Element methods to solve wave propagation problems, the spatial domain must be truncated at a finite distance. This can be done using absorbing boundary conditions or layers, which effectively inhibit the reflection of outgoing waves back into the computational domain. They cannot however handle moving loads coming from outside of the (truncated) computational domain, for which some incoming waves must be allowed. After illustrating this fact, this paper proposes a technique to introduce such moving loads in time simulations over finite size domains. This technique involves the introduction of appropriate initial conditions within the computational domain. In general, these initial conditions can be computed numerically, and possibly re-used for various configurations. The interest of the method is illustrated on industrial cases of interest for the railway community.

Keywords: Moving load, Wave Propagation, Time Domain Simulation, Finite Element Method, Railway engineering

2010 MSC: 00-01, 99-00

*Corresponding author

Email address: `cottereau@lma.cnrs-mrs.fr` (Régis Cottereau)

1. Introduction

When modeling the propagation of waves in unbounded media (for instance a half-space in railway-induced vibrations [1, 2, 3, 4, 5]) the use of traditional Finite Element Methods involves the truncation of the computational domain at a finite distance and the introduction of absorbing boundary conditions [6, 7] or absorbing boundary layers [8, 9, 10, 11] to prevent outgoing waves from bouncing back into the computational domain. We consider in this paper the excitation of such problems by moving loads, which often appear in engineering problems alongside invariance by translation (or periodicity) of the geometry, for instance to model the impact of passing vehicles in the vicinity of railway tracks [12, 13, 14], roads [5], tunnels [15], or pipelines [16] (see also [17] and references therein). When such is the case (or when the domain verifies that property in slices perpendicular to the loading support), these problems are efficiently solved in the frequency domain, either in the moving frame or in the periodicity cell [18, 15, 19, 20, 21]. However, anytime the geometry or the material parameters are neither invariant by translation nor periodic, these technique cannot be applied. Such situations include: a change of support structure (from a railway ballasted track to slab track for instance, which we will consider in the applications of Section 6), a change of supporting topography (a road arriving at a bridge for instance), a curve in the track (or road, tunnel, pipe), among others. As the locations of such changes of material properties and geometry are potential candidates for stress concentrations and increased strains, it is essential to be able to model them adequately. Time-domain simulations are then an interesting alternative to frequency-domain methods.

In this paper we illustrate that when applying a Finite Element method to solve problems with moving loads in the sub-Rayleigh regime (for which the charge moves at a speed lower than the Rayleigh wave speed in the ground) over unbounded domains, the truncation of the computational domain impacts the moving load very strongly. The most striking feature is the emission of a parasitic wave from the first point of application of the moving load. The

problem has been identified in the literature [22] and heuristic solutions [23, 24] have been proposed to qualitatively solve it, but with no clear explanation about its origin. Note that this issue is not so stringent for loads moving faster than the Rayleigh wave speed in the ground, so we will restrict our study to the
35 former case, which is also the case of interest for most railway applications. Note also that, in the absence of invariance by translation, the separation of the moving load into so-called quasi-static and dynamic excitations is meaningless.

The objective of this paper is two-folds: (i) explain precisely the reason why introducing bluntly a moving load in a truncated computational domain
40 induces a parasitic wave, and (ii) propose a technique to cancel that parasitic wave without increasing the computational cost. In Section 2 the problem of moving load studied in this paper is presented. In Section 3, a semi-analytical solution for the displacements induced by a moving load in an elastic half-space is presented. This solution allows us to explain clearly in Section 4 the origin
45 of the parasitic wave induced by the truncation of the computational domain. Section 5 answers the second objective of this paper by proposing to introduce non-homogeneous initial conditions to remove the parasitic wave. These initial conditions can be obtained by a preliminary simulation, potentially re-usable for different computational scenarii. Finally, in Section 6, two applications
50 in railway engineering highlight the interest and practicality of the proposed approach.

Note that the approach we propose bears some similarity with an existing technique [25]. As ours, this technique requires a preliminary simulation, but it packages the information of the moving load within displacement and traction
55 fields along an interface for all time steps (while our technique does so in a space volume, and only for one time step). Another important difference is that the referenced method requires the solver to handle discontinuous field, which is not possible with most classical (and commercial) solvers.

2. Equations of the wave field induced by a moving load

In this paper we assume $\mathbf{x} = (x, y, z)$ is a generic position in a Cartesian coordinate system. The displacement field in a domain Ω can be obtained by solving the equation of motion:

$$-\nabla \cdot \sigma(\mathbf{x}, t) + \mathbf{f}(\mathbf{x}, t) = \rho \frac{\partial^2 \mathbf{u}(\mathbf{x}, t)}{\partial t^2}, \quad (1)$$

where $\mathbf{f}(\mathbf{x}, t)$ is bulk force, $\mathbf{u}(\mathbf{x}, t) = (u, v, w)$ is the displacement vector, $\sigma = \lambda(\mathbf{x})\text{tr}\epsilon(\mathbf{x}, t)\mathbf{I} + 2\mu(\mathbf{x})\epsilon(\mathbf{x}, t)$ is the stress tensor (assuming linear elastic isotropic behavior for the material), $\epsilon(\mathbf{x}, t) = (\nabla \mathbf{u}(\mathbf{x}, t) + (\nabla \mathbf{u}(\mathbf{x}, t))^T)/2$ is the strain tensor, $\rho(\mathbf{x})$ is the density and $\lambda(\mathbf{x})$ and $\mu(\mathbf{x})$ are the Lamé parameters of the medium. We additionally define the pressure wave speed $C_P(\mathbf{x})$ and the shear wave speed $C_S(\mathbf{x})$ as:

$$C_P(\mathbf{x}) = \sqrt{\frac{\lambda(\mathbf{x}) + 2\mu(\mathbf{x})}{\rho(\mathbf{x})}}, \quad C_S(\mathbf{x}) = \sqrt{\frac{\mu(\mathbf{x})}{\rho(\mathbf{x})}}. \quad (2)$$

with $C_S(\mathbf{x}) < C_P(\mathbf{x})$, as well as the Rayleigh [26] wave speed $C_R(\mathbf{x}) < C_S(\mathbf{x})$, of importance for applications over half-spaces. The domain Ω is assumed to be unbounded, so that the equation of motion must be completed with Sommerfeld radiation conditions. When appropriate, for instance when Ω is a half-space, additional boundary conditions should be considered over the boundary at finite distance. For instance, and without limiting the scope of the derivation, we consider here Neumann boundary conditions on this boundary:

$$\sigma \cdot \mathbf{n} = \mathbf{g}(\mathbf{x}, t), \quad \mathbf{x} \in \partial\Omega. \quad (3)$$

Because the domain is unbounded, the computational approximation of Eq. (1) by traditional Finite Element Methods is completed with absorbing boundary layers [8, 9, 10, 11]. Finally, the equilibrium Eq. (1) and boundary conditions are completed with homogeneous initial conditions:

$$\mathbf{u}(\mathbf{x}, t = 0) = \mathbf{0}, \quad \frac{\partial \mathbf{u}}{\partial t}(\mathbf{x}, t = 0) = \mathbf{0} \quad (4)$$

In this paper we study the situation when the support of one of the loads, either $\mathbf{f}(\mathbf{x}, t)$ or $\mathbf{g}(\mathbf{x}, t)$, is unbounded, and is hence impacted by the truncation

of the computational domain. In particular, we will consider loads moving at a constant speed V along a line, in the form

$$\mathbf{f}(\mathbf{x}, t) = F_0(t)\delta(x - Vt)\delta(y)\delta(z)\mathbf{e}_z, \quad (5)$$

or, assuming that Ω is a half-space with a non-homogeneous Neumann boundary condition Eq. (3), with

$$\mathbf{g}(\mathbf{x}, t) = F_0(t)\delta(x - Vt)\delta(y)\mathbf{e}_z. \quad (6)$$

60 Here, the Dirac delta functions are defined for any smooth function $f(x)$ and position x_0 by $\int_{\mathbb{R}} \delta(x - x_0)f(x)dx = f(x_0)$. When the geometry and mechanical parameters of the system are invariant by translation, these problems can be easily solved in a frame moving with the load. Analytical solutions have been derived for instance for problems of moving bulk loads [27, 28] or for surface
65 loads at the boundary of half-spaces [29, 30, 31, 32, 33, 34, 35, 36].

3. Response of an elastic half-space due to a moving load

In this section, a semi-analytical solution of Eq. (1) over a half-space is proposed, where the moving load is applied over a set of equally-spaced points along a line [3] at the surface (see Fig. 1). This loading case is a discrete version
70 of a load moving continuously at the surface of a homogeneous half-space along a line, for which analytical solutions exist [30, 31, 32, 33, 34, 37]. The reason for considering this discrete force model is mainly that it will be easier to illustrate the impact of truncating the computational domain in Section 4. Also, discrete load models are actually closer to the real situation than continuous moving
75 loads in many engineering applications. This is for instance the case of railway applications, where loads are transmitted from the train/track system to the ballast through sleepers, separated by a distance d . Each sleeper can be seen as a separate dynamic load for the ground, firing with a time lag of d/V with respect to its neighbors, where V is the velocity of the train. Even though the
80 presentation considers a discrete load, the analysis as well as the conclusions of

the paper would remain identical in the alternative case of a moving load with continuous support.

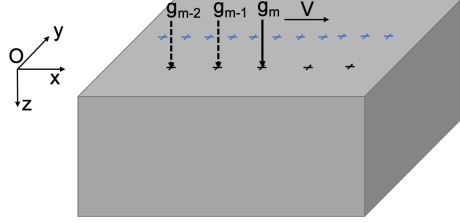


Figure 1: A constant force moving at the surface of a homogeneous half-space and applied at a discrete set of points (black crosses) along a line. Sensors (blue crosses) are located along a line parallel to the load line.

Let us consider a normal load, moving with a uniform velocity V over a set of equally-spaced points along a line ($y = 0, z = 0$) at the surface of a half-space bounded by $z = 0$, as in Eq. (6). The problem is described on Fig. 1. We assume that the medium is elastic, isotropic and homogeneous. The Neumann boundary condition (Eq. (3) with $\mathbf{n} = -\mathbf{e}_z$) at the surface of a half-space is constituted of a sum of traction forces centered on positions $x = md$ and times $t - md/V$, $m \in \mathbb{Z}$:

$$\forall m \in \mathbb{Z}, \quad \mathbf{g}_m(\mathbf{x}, t) = F_0 \left(t - \frac{md}{V} \right) \delta(x - md) \delta(y) \mathbf{e}_z, \quad (7)$$

such that

$$\mathbf{g}(\mathbf{x}, t) = \sum_{m \in \mathbb{Z}} \mathbf{g}_m(\mathbf{x}, t). \quad (8)$$

As the vibration energy at the surface of a homogeneous half-space is mostly transmitted by the surface waves [38], Krylov [3] computed the spectrum of the vertical displacements for the Rayleigh surface wave contribution induced in the far field at the surface ($z = 0$) of a homogeneous half-space by such a boundary condition:

$$w(x, y, \omega) = F_0(\omega) D(\omega) d \sum_{m=-\infty}^{\infty} \frac{\exp(i(\omega/V)md + ik_R(\omega)r_m)}{\sqrt{r_m}} \quad (9)$$

where $r_m = \sqrt{(x - md)^2 + y^2}$ is the distance between each source and the observation point, $k_R(\omega) = \omega/C_R(\omega)$ is the wavenumber of the Rayleigh surface

wave,

$$D(\omega) = \frac{1}{\sqrt{2\pi}} \sqrt{k_R^2 - k_P^2} \sqrt{k_R k_S^2} \frac{\exp(-i3\pi/4)}{\mu(\omega) Q'(k_R)}, \quad (10)$$

$k_P = \omega/C_P$ and $k_S = \omega/C_S$ are the wavenumbers of the pressure and shear waves, and $Q'(k)$ is the derivative of the dispersion equation of Rayleigh waves:

$$Q(k) = (2k^2 - k_S^2)^2 - 4k^2 \sqrt{k^2 - k_S^2} \sqrt{k^2 - k_P^2}. \quad (11)$$

Note that the amplitude d in front of Eq. (9) has been added to allow comparison between load cases with different spacings.

85 An example of a load $F_0(t)$ (see below) moving at a constant speed $V = 90$ m/s on a homogeneous half space with velocities $C_P = 600$ m/s, $C_S = 450$ m/s, $C_R = 380$ m/s and density $\rho = 1800$ kg/m³ is considered. Displacement fields obtained using discrete version of a loading are presented for different values of d . The load $F_0(t)$ considered is an impulse applied on the
 90 ground and containing frequencies in the band 10-100Hz. The time representation of the load and its frequency content are presented in Fig.2. The same parameters for the medium and load will be re-used later in this paper.

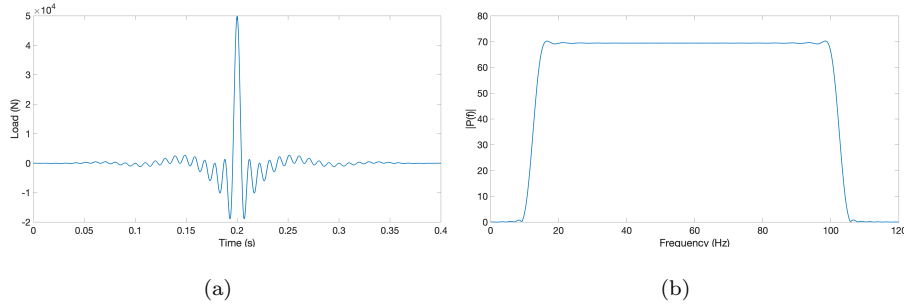


Figure 2: Time history (a) and spectrum (b), of the excitation $F_0(t)$.

Fig. 3 presents displacements induced in the soil ($x = 0$ m, $y = 2$ m, $z = 0$ m) for $d = 0.1$ m and $d = 0.6$ m (typical of railway tracks in France) obtained with
 95 Eq. (9) by considering a sum from $m = -2500$ to $m = 2500$, which represents a domain of length $5000d$. Note that considering this range for the sum means that point loads very far from the sensors are considered. For $d = 0.6$ m, a

similar pattern is observed as for $d = 0.1$ m, with additional waves before and after the passage of the load. Indeed, a moving load on a discrete set of points
 100 generates propagating waves in the ground for both sub-Rayleigh regime and trans-Rayleigh regime [39], although interferences between the different sources eventually lead for smaller distances to the disappearance of any significant amplitude at a distance from the source positions. However when the distance d increases the pattern of the displacement changes and waves after the passage of the load are present (see displacements in Fig. 4 obtained with $d = 1$ m).

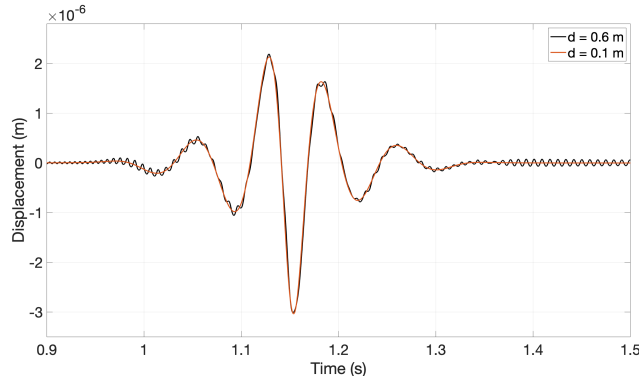


Figure 3: Vertical displacements in the soil ($x = 0$ m, $y = 2$ m, $z = 0$ m) for different spacings between two consecutive loads: $d = 0.1$ m (orange solid line) and $d = 0.6$ m (black solid line). The length of the domain is $5000d$.

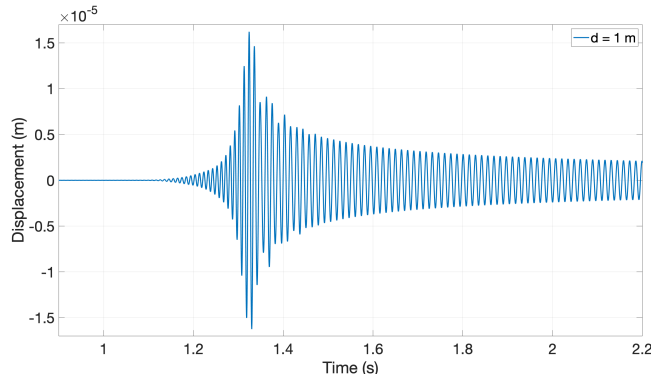


Figure 4: Vertical displacement in the soil ($x = 0$ m, $y = 2$ m, $z = 0$ m) for a spacing $d = 1$ m between two consecutive loads. The length of the domain is $5000d$.

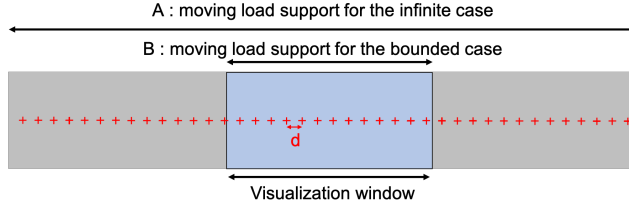


Figure 5: Visualization window of displacements for (A) the infinite case and (B) for the finite case of the moving load support. Crosses represent the excitation points.

105 Fig. 6 presents the vertical displacements induced by a discrete load with spacings $d = 0.1$ m for sensors between positions $(x, y, z) = (0, 2, 0)$ m and $(x, y, z) = (100, 2, 0)$ m (case A on Fig. 5), along a line parallel to the loading line (see the blue crosses in Fig. 1). This line is located 2 m from the loading line. As discussed above, the response of the half-space is mainly composed of
 110 evanescent waves. It means that there are no waves generated along the line force and propagating away from it. There is only a stationary displacement field whose support is localized in the vicinity of point of application of the load and moving along with that load.

4. Parasitic waves induced by the limited extent of the spatial support 115 of the moving load

In this section, we investigate what happens when a moving load coming from outside a truncated computational domain enters that domain. The boundedness of the computational domain induces that of the support of the moving load and generates parasitic waves where that support intersects the boundary
 120 of the computational domain. The appearance of these parasitic waves will be shown in the semi-analytical case of Section 3 and for a Finite-Element type numerical simulation, in Sections 4.1 and 4.2, respectively. This issue has already been observed in the literature, although not explained precisely, and Section 4.3 discusses a technique that was introduced to mitigate it, highlighting its limits

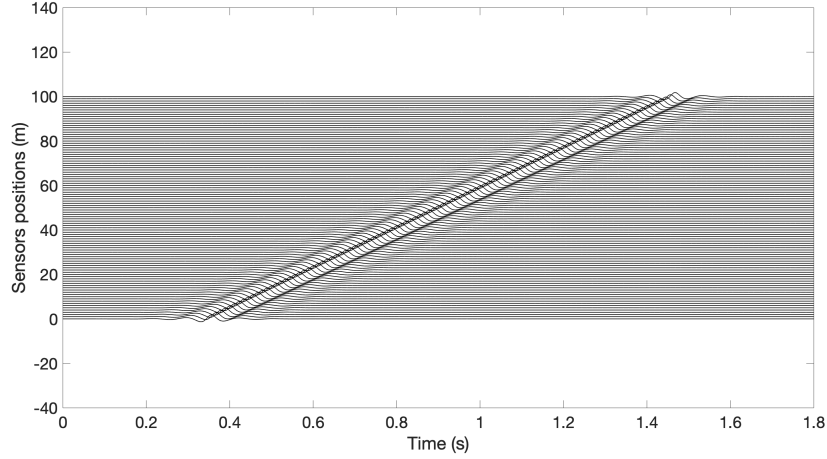


Figure 6: Vertical displacements induced by a discrete load with $d = 0.1$ m obtained with semi-analytical solution, at sensors along a line parallel to and 2 m away from the loading line. The domain is of length 500 m.

125 before proposing an alternative approach in Section 5.

4.1. Impact of domain truncation on the vibrations induced by a discrete moving load in the semi-analytical case

We consider the load of Section 3, but this time with only a finite number N of discrete loads, mimicking the boundedness of a computational domain. The displacement field in a given (x, y, z) sensor is therefore obtained as a finite sum, counterpart of Eq. (9):

$$w(x, y, \omega) = F_0(\omega)D(\omega)d \sum_{m=-N}^N \frac{\exp(i(\omega/V)md + ik_R(\omega)r_m)}{\sqrt{r_m}} \quad (12)$$

Displacements obtained for $N = 500$ with $d = 0.1$ m, which correspond to loads between $x = 0$ m and $x = 100$ m (case B on Fig. 5), are presented on Fig. 7. In the center of Fig. 7, we retrieve the quasi-static displacements induced by the moving load, and moving with its velocity V , already identified in Fig. 6. However, compared to Fig. 6, there are two additional propagating waves. These waves propagate at the velocity of the waves in the soil C_R and are generated at the boundaries of the loading support, at positions $x = 0$ and

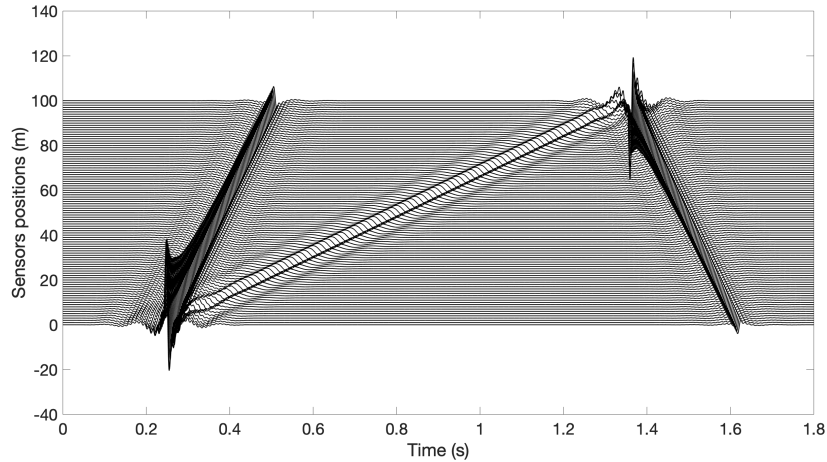


Figure 7: Vertical displacements induced by a moving load over a bounded series of points obtained with semi-analytical solution, at sensors located along a line parallel to and 2 m away from the loading line. The length of the domain is 100 m.

135 $x = 2Nd$. What happens is that the quasi-static appearance of the displacement induced by the unbounded load actually arises as a complex interference between waves coming from the different sources. In the middle of the loading line, this interference can take place normally. However, on the boundaries of the loading line, the sources outside the computational domain are lacking. The absence
 140 of the corresponding waves means that full interference cannot take place. The waves emitted from the first and last few sources are therefore not properly compensated and reappear as propagating waves in the soil.

4.2. Numerical simulation of a moving load over a truncated half-space

In this section, we illustrate exactly the same effect, but with a 3D Spectral
 145 Element Method software presented in Appendix A, rather than the above semi-analytical model.

The homogeneous half-space with the same mechanical properties as in the Section 3 is represented by a box of dimensions 40 m \times 100 m \times 10 m, as illustrated on Fig. 8. Perfectly Matched Layers are used on the exterior of the
 150 box to absorb outgoing waves. There are 75 layers of PML with a total thickness

of 60 m. The load presented in Fig. 2 is moving at a constant velocity along a line at the surface of the soil (black line on Fig. 8). The distance between two application points is $d = 0.1$ m. The mesh size goes from $h = 0.4$ m, close to the points of application of the load, to $h = 0.8$ m away from it.

155 There are around 5.9×10^6 hexahedral elements, with **5 nodes** in each direction (tensorization of **4th-order** polynomials in each space dimension) for a total of **375 degrees of freedom** per element in 3D. The time step is 1.8×10^{-5} s.

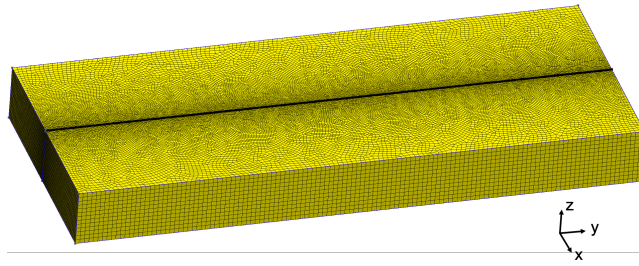


Figure 8: Geometry of the homogeneous half-space. Perfectly Matched Layers are not represented.

Displacements induced in the soil at sensors along a line parallel to the loading line and at 2 m from it are presented in Fig. 9. Note that the model

160 aims at mimicking that of Section 3, so that the results of Fig. 9 are expected to match those of Fig. 6, for $d = 0.1$ m. But as the loading cannot be modeled outside of the computational domain, we actually retrieve the results of Section 4.1 and Fig. 7, with a parasitic wave emitted at the boundaries of the loading line, where the waves emitted from outside the computational domain

165 are missing and cannot create the correct interference patterns.

In conclusion, when considering a bounded support to approximate a moving load over an unbounded line, waves are generated at the boundaries of that support. These are parasitic waves in the sense that they do not appear in the reference model (for unbounded support). Their presence strongly pollutes the

170 numerical simulation (see Section 6.1 for a striking example of that pollution) and they have to be removed in order for the simulation to provide meaningful

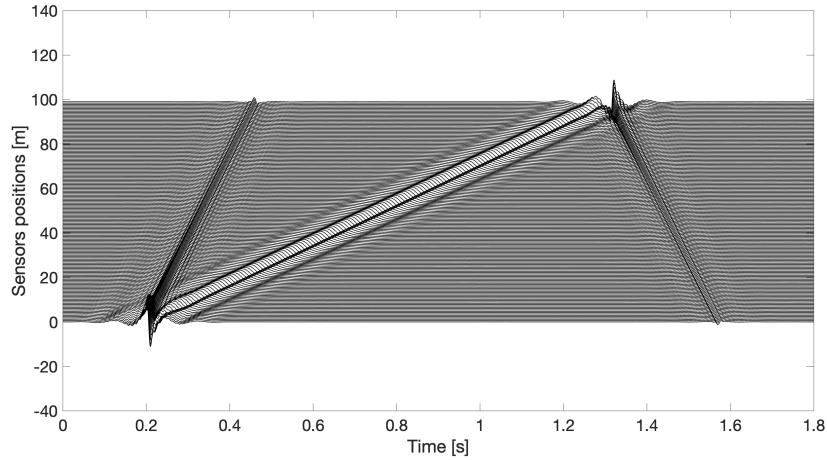


Figure 9: Vertical displacements induced by a moving load, computed using a SEM solver at sensors located along a line parallel to and 2 m away from the loading line. The length of the domain is 100 m.

results. Note that, in the simulations shown above, if the velocity of the moving load V approaches that of the Rayleigh wave C_R , the parasitic wave may pollute the physical wave over large distances, which means the simulation would need
 175 to run over a very large domain (and over very long times) in order for the computational result to be accurate.

4.3. Influence of introducing the loading gradually in a numerical simulation

The generation of such parasitic waves has already been observed in the literature. For instance, this problem was mentioned in [22] although no solu-
 180 tion was proposed. As a mitigation, it is sometimes proposed to progressively increase the velocity and magnitude of the loading from an initial zero up to the desired velocity. However, this technique either requires a lot of additional ressources (larger computational domain and longer simulation times) or only partially solves the issue.

We use here the particular proposal of [23], who applied a load as in Eq. (6), but with a time-varying amplitude and velocity. We choose to apply the ampli-

tude $F_0(t)$ and the velocity $V(t)$ as follows :

$$F_0(t) = \begin{cases} \frac{t}{T_{\text{acc}}} F_0^* & \text{if } t < T_{\text{acc}} \\ F_0^* & \text{if } t \geq T_{\text{acc}} \end{cases}, \quad V(t) = \begin{cases} \frac{V^*}{T_{\text{acc}}} t & \text{if } t < T_{\text{acc}} \\ V^* & \text{if } t \geq T_{\text{acc}} \end{cases} \quad (13)$$

185 where F_0^* and V^* are the target amplitude and velocity, that are attained after an initial acceleration phase of duration T_{acc} . Below, we show examples with the same problem as in the previous sections but introducing this time the load for different initial acceleration times T_{acc} . The soil is represented by a larger box of new dimensions 40 m \times 122.5 m \times 10 m. There are 88 layers of PML with
 190 a total thickness of 70 m. The mesh is composed of about 8.2×10^6 hexahedral elements with **5 nodes** and a size $h = 0.8$ m in each direction. The time step is 2.2×10^{-5} s. We expect the solutions to resemble that of Fig. 6.

We first consider an acceleration of the load in the initial phase of $V^*/T_{\text{acc}} = 450$ m/s² and plot the corresponding displacements at sensors located along a
 195 line parallel to and 2 m away from the load line in Fig. 10. The amplification and the progressive acceleration of the load allow to decrease the magnitude of the parasitic waves generated when the load is introduced. However at time $t = 0.4$ s, a parasitic wave is still observed, generated at the moment when the load reaches the target velocity V_{target} . Furthermore, such an acceleration
 200 requires to create a larger computational domain (approximately 10 m here), and longer simulation times (approximately 0.15 s here) in order to accommodate a given time-space frame of interest.

Fig. 11 presents similar results for a load introduced even more slowly, with $V^*/T_{\text{acc}} = 180$ m/s². As expected, the amplitude of the parasitic wave is even
 205 more reduced, almost vanishing, but the computational domain and simulation time would need to be even larger (approximately 20 m and 0.3 s here) in order to accommodate a given time-space frame of interest.

The progressive introduction of the load therefore allows to solve the problem of the parasitic waves arising from the truncation of the load support. However,
 210 it comes at the cost of a requirement to increase the computational domain and simulation time, which can rapidly be an issue for large scale simulations,

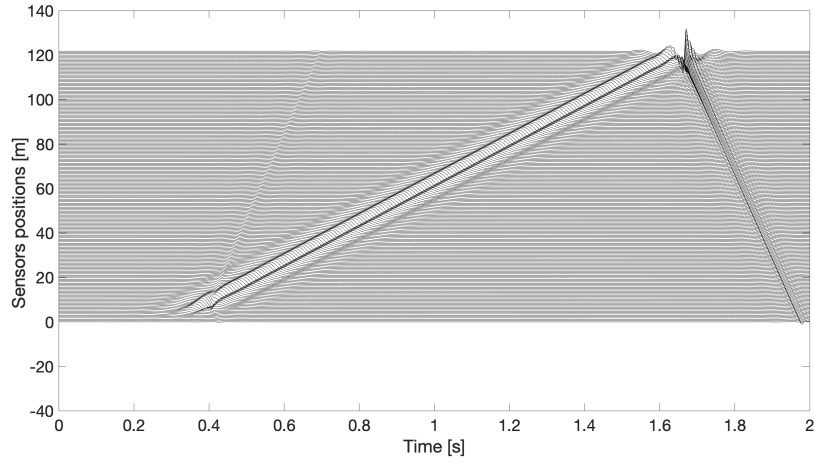


Figure 10: Vertical displacement induced by an accelerating ($V^*/T_{acc} = 450 \text{ m/s}^2$) moving load at sensors placed along a line parallel to and 2 m away from the loading line. The length of the domain is 122 m.

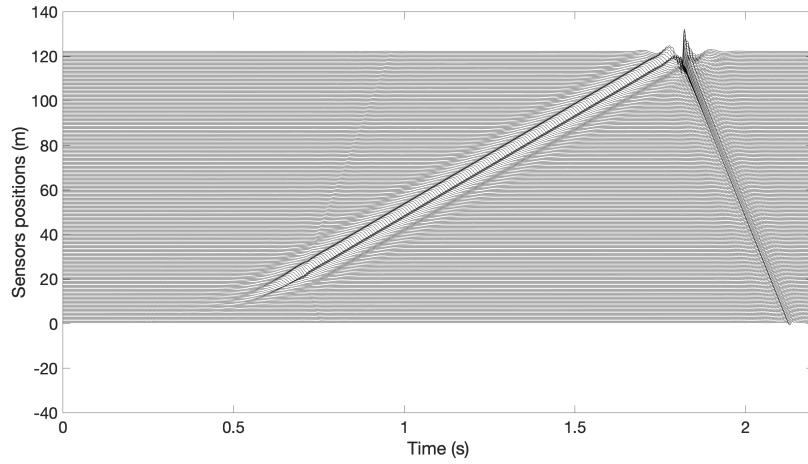


Figure 11: Vertical displacement induced by an accelerating ($V^*/T_{acc} = 180 \text{ m/s}^2$) moving load at sensors placed along a line parallel to and 2 m away from the loading line. The length of the domain is 122 m.

that are already very costly. In next section, we propose a technique to remove that parasitic wave, with no need to increase the computational domain or the simulation time. Note that the parasitic wave at the end of the simulation is not

215 removed (as will also be the case with our technique) but this is not necessarily
an issue as the simulation often stops when the loads exists the computational
domain.

5. Spectral Element Method with non homogeneous initial conditions

5.1. General idea

220 The solution of a wave equation is uniquely defined by its initial conditions.
So solving the original problem of Eq. (1) on an unbounded domain (for example,
the blue domain in the Fig. 12) is the same as solving it in a smaller domain (for
example, the box in the Fig. 12), as long as the support of the initial conditions
is enclosed completely within that small domain. The general idea of the paper
225 therefore consists in decomposing a given time simulation into two steps:

1. A preliminary simulation to compute the stationary state $\mathbf{u}_0(\mathbf{x}, t = T)$
and $\mathbf{v}_0(\mathbf{x}, t = T)$, removing the influence of any parasitic wave;
2. The simulation of interest using these fields as non-homogeneous initial
conditions $\mathbf{u}(\mathbf{x}, t = 0) = \mathbf{u}_0(\mathbf{x}, t = T)$ and $\mathbf{v}(\mathbf{x}, t = 0) = \mathbf{v}_0(\mathbf{x}, t = T)$, free
230 of parasitic wave.

The idea is to separate the parasitic wave from the true wave in the results of a
simulation as featureless as possible. Devoid of most reflectors and interfaces of
the simulation of interest, the separation becomes possible in a smaller domain
and shorter time. The simulation of interest can then be performed with no
235 parasitic wave, by encapsulating the information about all previous loadings
within the initial conditions.

In addition, this decomposition allows to re-use the same initial state for
several simulations of interest (as will be shown in the examples of Section 6).

5.2. Preliminary simulation

240 The preliminary simulation consists in considering a domain Ω_0 , similar to
the original domain Ω around the position where the moving load enters the
computational domain. The domain Ω_0 (and the properties) must be chosen to

ensure that a stationary solution can be obtained, and which then represents the initial conditions for the simulation of interest. In particular, any obstacle that might inhibit parasitic waves from exiting the domain should be removed. For example, for the case of a transition zone (detailed in Section 6), from ballast to concrete, a translation-invariant ballasted track (with no transition to concrete) will be considered for the preliminary simulation.

The following problem is then approximated as:

$$-\nabla \cdot \sigma_0(\mathbf{x}, t) + \mathbf{f}(\mathbf{x}, t) = \rho \frac{\partial^2 \mathbf{u}_0(\mathbf{x}, t)}{\partial t^2}, \quad \mathbf{x} \in \Omega_0, t \in [0, T]. \quad (14)$$

At some time τ , the solution reaches a stationary state for which $\mathbf{u}_0(\mathbf{x} + Vt, \tau + t) = \mathbf{u}_0(\mathbf{x}, \tau)$ for all $t > \tau$ (remember that V is the load velocity). These stationary displacement and velocity fields $\mathbf{u}_0(\mathbf{x}, \tau)$ and $\mathbf{v}_0(\mathbf{x}, \tau)$ are then collected.

In particular cases, such stationary fields are known analytically (see the references in the introduction), but in general they have to be estimated numerically. For instance, Fig. 12 presents the displacement field $\mathbf{u}_0(\mathbf{x}, \tau)$ computed at $\tau \approx 1$ s for the geometry and loading seen in Section 4.2. A box of dimensions $30 \text{ m} \times 40 \text{ m} \times 5 \text{ m}$ is chosen (indicated in black on Fig. 12), within which displacements and velocities are exported. The box is chosen large enough so that the fields are sufficiently close to zero at the boundaries.

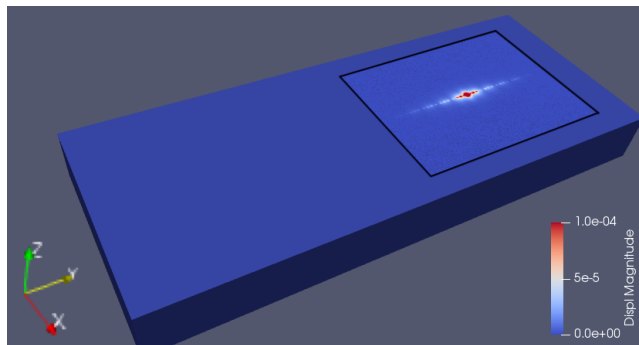


Figure 12: Final displacements (plotted) and velocities are extracted from the simulation in order to be used as initial conditions in a future simulation. Displacements inside the Perfectly Matched Layers are not represented.

We are essentially assuming here that the displacement and velocity fields reach a stationary state. Although it is not possible to give a clear definition of the class of problems that may verify this property, it is expected that this is the case at least for problems where the geometry and the properties are invariant by translation along a direction parallel to that of the loading. This situation is very common in industrial applications. Note that this condition applies only to the preliminary simulation, and not to the simulations of interest.

5.3. Simulation of interest

Coming back to the simulation of interest, the following problem is then solved, on the original domain Ω :

$$\begin{cases} -\nabla \cdot \boldsymbol{\sigma}(\mathbf{x}, t) + \mathbf{f}(\mathbf{x}, t) = \rho \frac{\partial^2 \mathbf{u}(\mathbf{x}, t)}{\partial t^2}, & \mathbf{x} \in \Omega, t \in [0, T], \\ \mathbf{u}(\mathbf{x}, t = 0) = \mathbf{u}_0(\mathbf{x} - \mathbf{x}_0, \tau), \\ \mathbf{v}(\mathbf{x}, t = 0) = \mathbf{v}_0(\mathbf{x} - \mathbf{x}_0, \tau), \end{cases} \quad (15)$$

where \mathbf{x}_0 is chosen so that the initial conditions and loading $\mathbf{f}(\mathbf{x}, t = 0)$ align properly.

Although it bears little interest in practice, Fig. 13 presents the displacement field of interest obtained when the domain, boundary conditions and properties are the same as for the preliminary simulation. More interesting applications will be presented in Section 6 and the main interest of this application is to show that the initial parasitic wave due to the truncation of the computational domain is completely suppressed with the non-homogeneous initial conditions.

5.4. Potential issues with interpolation of the initial conditions

In general, an interpolation step is required to obtain the initial conditions of the simulation of interest from the fields extracted at the end of the preliminary simulation. For low-order Finite Element methods, linear interpolation works fine. However, when using high-order Finite Element methods, the interpolation step may be more tricky numerically, in particular with unstructured meshes, because that interpolation has to consider the basis functions really used for the

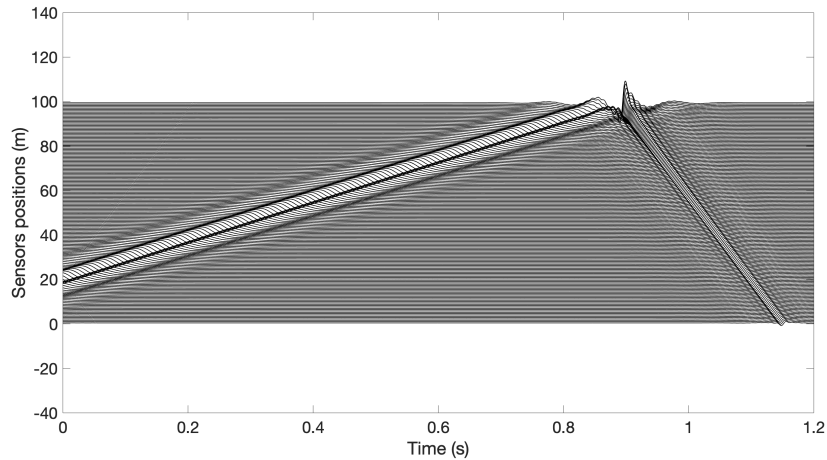


Figure 13: Vertical displacements induced by a moving load, computed using a SEM solver with non-homogeneous initial conditions, at sensors located along a line parallel to and 2 m away from the loading line. The length of the domain is 100 m.

particular method. However it is still possible to use linear interpolation if the elements are small enough (and the time scheme has good spectral properties) to ensure that the interpolation error does not mix with the frequency range
 285 of interest. In that case a simple *a posteriori* low-pass filtering can remove the high-frequency errors without modifying the solution of interest. This is what was implemented for the purpose of the examples presented in this draft, with a filter removing all frequencies above 300 Hz. The filter used was a zero-phase filter [40] *filtfilt* available in Matlab.

290 6. Applications to railway engineering

In this section two examples of railway application are presented. The first example considers a bogie arriving in the vicinity of a trench while the second example considers a transition area, where the ballasted railway track is replaced by a slab track, with very different mechanical properties of the structure supporting the rails. Beside their own interest, these two examples aim at
 295 showing that the initial conditions can be re-used for different computational

scenarii. We will therefore assume that the initial setting is the same for both simulations, with a simple model of the track where only the soil and the ballast layer are taken into account (the rails are not modeled). The soil is assumed

300 linear, elastic and homogeneous with pressure wave velocity $C_P = 600$ m/s, shear wave velocity $C_S = 350$ m/s and density $\rho = 1800$ kg/m³. The ballast is also linear, elastic and homogeneous with $C_P = 397$ m/s, $C_S = 212$ m/s and $\rho = 1700$ kg/m³. The 3D model for the computation of the initial conditions is presented in Fig. 14 (upper right). The load considered is that induced by a bogie on a typical railway track, estimated with the approach of [41] where the rail

305 is modeled as an Euler-Bernoulli beam with a section stiffness $EI = 6.3$ MNm² and a mass per unit length $\rho S = 60$ kg/m. It is periodically supported by supports separated by a distance $l = 0.6$ m. The stiffness of the support system is assumed to be equal to $k_s = 192$ MNm⁻¹. The time dependence of the loading is presented in Fig. 15. The load is moving with a speed $V = 90$ m/s and is applied on the ballast every $d = 0.1$ m. The height of the ballast layer is 0.9 m, the width on the ground is 8 m and that at the top of the layer is 6 m. It is modeled with elements of size 0.4 m. The soil is represented by a box of dimensions 20 m \times 4 m \times 96.3 m with a mesh size increasing from 0.4 m to

315 1 m. This box is surrounded on five sides by PMLs with a thickness of 60 m. The total number of elements is around 5.7×10^6 for a total of **375 degrees of freedom per element in 3D (5 nodes in each direction)**. The simulation of 0.96 s requires 9h of calculation on 512 processors with a time step of 1.5×10^{-5} s. The displacement and the velocity fields are saved at the time $T = 0.95$ s in a

320 box of size 12 m \times 4.9 m \times 65 m (blue box on Fig. 14 (upper right)).

In order for a single set of initial conditions to be used for simulations with different geometries (domains), it is necessary that all the conditions prior to arriving on the zone of interest (in the simulation of interest) are the same as those used in the preliminary simulation to determine initial conditions. In the

325 example given in this section, the two simulations start when the bogie stands in an area where both geometry (no trench) and material properties (ballast layer over soil) are the same. Only in the zones of interest (when the bogie

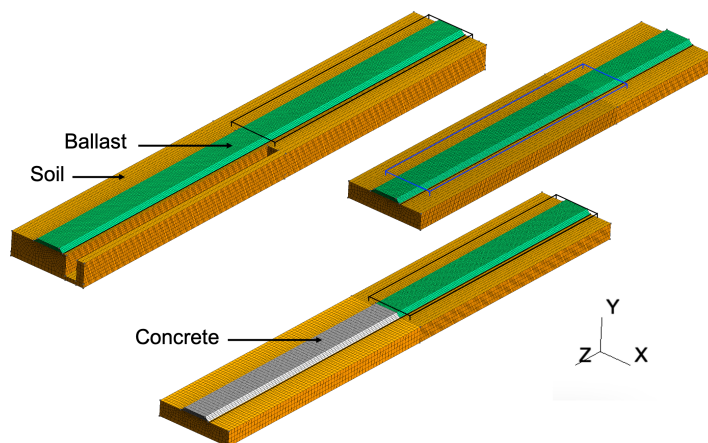


Figure 14: 3D models of railway track: ballasted railway track for the application with a trench (upper left), ballasted railway track for the computation of initial conditions (upper right), and railway track with a transition from a ballasted track to a slab track (down). The boxes indicate where the initial conditions were obtained (blue box) and where they are introduced in the simulations of interest (black boxes). Sensors are located along a line (black line) parallel to and 10 cm away from the ballast. Perfectly Matched Layers are not represented.

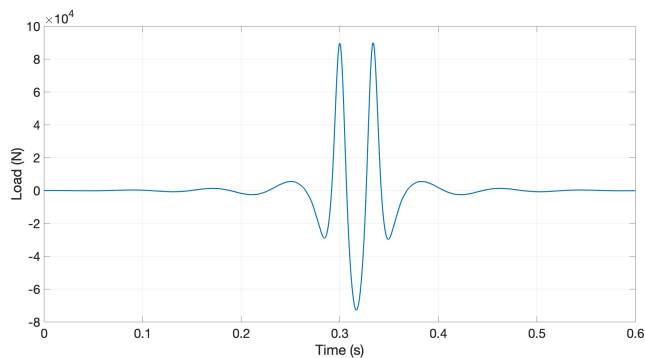


Figure 15: Time dependence of the bogie load

arrives at the height of the trench for the application of Section 6.1; and at the ballast-concrete transition for the application of Section 6.2) do the models change.

330

6.1. Train pass-by on a homogeneous half-space with a trench

In this section, the initial conditions presented above are used to simulate a bogie arriving in the area where a trench has been dug. The trench is 3 m wide, 5 m deep and located at 1 m from the ballast. Because the trench is rather far
335 away from the track, the trench should not have any effect on the wave field. However, we expect that, if not properly treated, the parasitic wave completely destroy the interest of the simulation because it bounces off the edge of the trench. The size of the box representing the soil is $20 \text{ m} \times 4 \text{ m} \times 132.3 \text{ m}$. The 3D model with a total of 6.2×10^6 hexahedral elements is presented on Fig. 14
340 (upper left). The simulation of 0.86 s with initial conditions requires 15 h of calculation on 256 processors with a time step of 1.2×10^{-5} s.

The displacements in the soil along a line parallel to and 10 cm away from the ballast are presented in Fig. 16 for the case when vanishing initial conditions are considered and in Fig. 17 for the case with initial conditions obtained as described above. We can clearly observe on the first simulation that the numerical
345 results are polluted not only by the parasitic waves but also by their reflections at the edge of the trench. The results with initial conditions on the other hand show no influence of the trench, as expected. The use of initial conditions is therefore absolutely unavoidable in order to obtain a correct estimation of the displacements induced by the passage of the train. The method proposed in
350 this paper allows to obtain the correct displacement field in an efficient manner.

6.2. Train pass-by on a transition zone between ballasted track and slab track

In this second application, we consider a transition area, where the ballasted railway track becomes a concrete slab track. As ballast and concrete
355 have different mechanical properties, waves are expected to be generated at the interface. The concrete is assumed homogeneous with pressure wave velocity $C_P = 3725 \text{ m/s}$, shear wave velocity $C_S = 2236 \text{ m/s}$ and density $\rho = 2400 \text{ kg/m}^3$. The total length of the track is 123.3 m, with 66 m of ballasted track and 66.3 m
360 of concrete slab. The mesh size in the concrete varies between 0.4 m and 1 m.

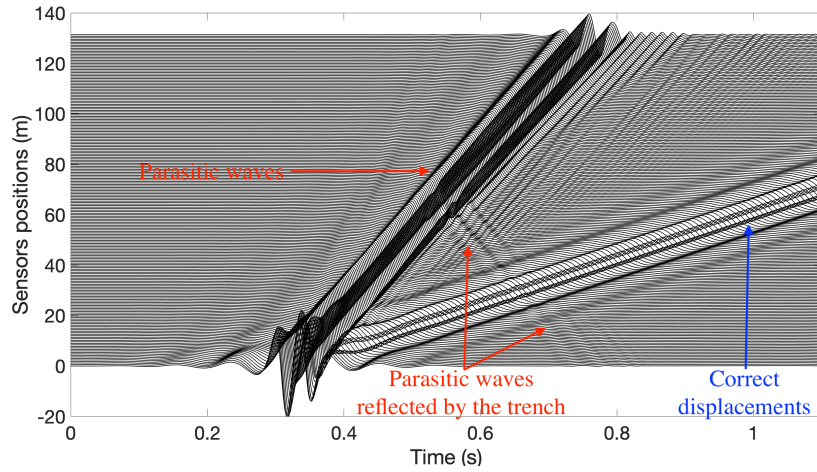


Figure 16: Vertical displacement induced in the soil by a moving load at 10 cm from the ballast layer.

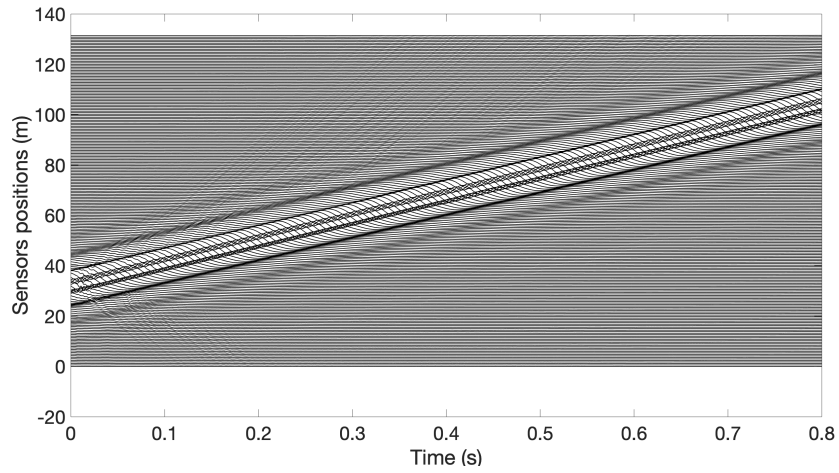


Figure 17: Vertical displacement induced in the soil by a moving load for sensors along a line parallel to and 10 cm from away the ballast layer after introduction of initial conditions.

The PMLs in contact with the concrete have a thickness of 250 m. The soil and ballast are meshed in the same way as in the previous section. The 3D model with a total of around 5.8×10^6 elements is presented in Fig. 14 (down). The simulation of 0.96 s requires 45 h of calculation on 512 processors with a time

365 step of 2.8×10^{-6} s.

The displacements in the soil are presented in Fig. 18. We indeed observe a wave propagating away from the transition. As the mechanical properties of the problem are not invariant by translation, it is interesting to note that the classical computational approaches (in particular in the frequency domain) cannot be used. Again, the method yields the expected result in an efficient manner.

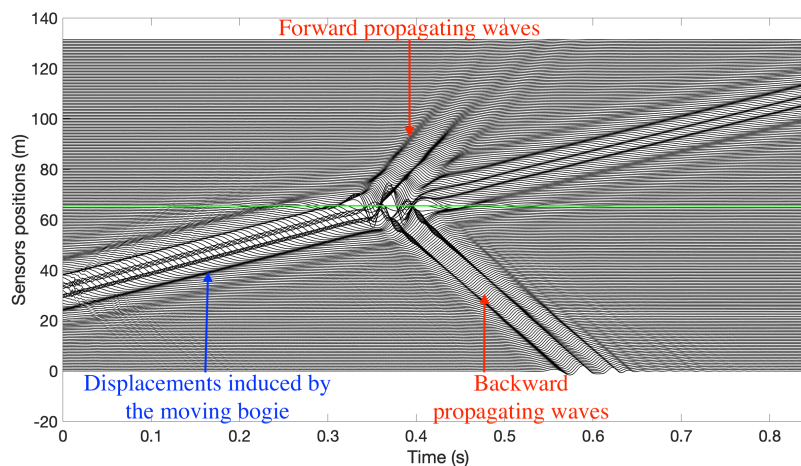


Figure 18: Vertical displacement induced in the soil by a moving load over a transition area, at sensors located along a parallel line to and 10 cm from away the ballast. The green line indicates the position of the transition from ballasted track to slab track.

7. Conclusion

A load moving at a sub-Rayleigh speed on an unbounded half-space generates an evanescent wave front located in the vicinity of the load. When solving such problems with the Finite Element Method in time, the truncation of the computational domain induces the generation of parasitic waves at the boundaries of the support of the moving load. The origin of these parasitic waves is a missing destructive interference: the waves supposedly coming from outside the computational domain are lacking so that waves that should have been destroyed

380 are then emitted away from the load. After demonstrating clearly through analytical and numerical examples the origin of these parasitic waves, the paper proposed a technique to remove them. It consists in introducing non-vanishing initial conditions in the simulation. These initial conditions can be computed using an independent and preliminary simulation, and possibly re-used for different computational scenarii (this was illustrated in Section 6). Re-using these preliminary simulations can be very convenient in the context of industrial applications, where track geometry and properties are mostly normalized. It can be also useful in the context of inverse problems or reliability analyses, where multiple runs have to be performed with potentially the same initial conditions. 390 The main requirement for this technique to work is that the initial conditions (not the simulation of interest) correspond to some stationary type of solution, as for instance that reached by a moving load on a homogeneous half-space or on any translation-invariant geometry. In particular, for non-linear soil behavior, when such stationarity can be reached, the technique is still expected to work.

395 **8. Acknowledgements**

The authors would like to thank Etienne Balmès for interesting discussions on this topic. Simulations were performed on SEM3D, a Spectral Element solver jointly developed by MSSMat Laboratory (CentraleSupélec, CNRS and Université Paris-Saclay), Institut de Physique du Globe de Paris (Paris Institute of Earth Physics) and the Commissariat à l'Énergie Atomique et aux énergies alternatives (French Atomic Energy Commission). Centre de Calcul Intensif 400 d'Aix-Marseille is acknowledged for granting access to its high performance computing resources.

Appendix A.

405 SEM3D software is a High-Performance Computing software based on the Spectral Element Method [42] (SEM) and co-developed by MSSMat Laboratory (CentraleSupélec, CNRS and Université Paris-Saclay), Institut de Physique

du Globe de Paris (Paris Institute of Earth Physics) and the Commissariat à l'Énergie Atomique et aux énergies alternatives (French Atomic Energy Commission), used for instance in [43, 44, 45, 46, 47]. The SEM is a Finite Element Method that uses Lagrange polynomials based on the nodes of the Gauss-Lobatto-Legendre quadrature and integrates numerically the weak formulation using that same quadrature. This leads to a diagonal mass matrix which allows to construct a very efficient explicit time scheme and yield very efficient parallelization.

- [1] X. Sheng, C. Jones, M. Petyt, Ground vibration generated by a load moving along a railway track, *Journal of sound and vibration* 228 (1) (1999) 129–156.
- [2] P. Zoccali, G. Cantisani, G. Loprencipe, Ground-vibrations induced by trains: Filled trenches mitigation capacity and length influence, *Construction and Building Materials* 74 (2015) 1–8.
- [3] V. Krylov, Generation of ground vibration boom by high-speed trains. in: Krylov, vv (ed.). *noise and vibration from high-speed trains* (2001).
- [4] G. Lombaert, G. Degrande, Ground-borne vibration due to static and dynamic axle loads of intercity and high-speed trains, *Journal of Sound and vibration* 319 (3-5) (2009) 1036–1066.
- [5] G. Lombaert, G. Degrande, D. Clouteau, Numerical modelling of free field traffic-induced vibrations, *Soil Dynamics and Earthquake Engineering* 19 (7) (2000) 473–488.
- [6] D. Givoli, High-order local non-reflecting boundary conditions: a review, *Wave Motion* 39 (4) (2004) 319–326. doi:10.1016/j.wavemoti.2003.12.004.
- [7] F. Magoulès, I. Harari, Absorbing boundary conditions, *Computational Methods in Applied Mechanics and Engineering* 195 (29-32) (2006) 3551–3902.

- [8] J.-P. Berenger, A perfectly matched layer for the absorption of electromagnetic waves, *Journal of Computational Physics* 114 (2) (1994) 185–200. doi:10.1006/jcph.1994.1159.
- [9] G. Festa, J.-P. Vilotte, The Newmark scheme as velocity-stress time-staggering: an efficient PML implementation for spectral element simulations of elastodynamics, *Geophysical Journal International* 161 (2005) 789–812.
- [10] A. Modave, E. Delhez, C. Geuzaine, Optimizing perfectly matched layers in discrete contexts, *International Journal for Numerical Methods in Engineering* 99 (2014) 410–437. doi:10.1002/nme.4690.
- [11] S. François, H. Goh, L. F. Kallivokas, Non-convolutional second-order complex-frequency-shifted perfectly matched layers for transient elastic wave propagation, *Computational Methods in Applied Mechanics and Engineering* 377 (113704) (2021) 1–23. doi:10.1016/j.cma.2021.113704.
- [12] C. Madshus, A. M. Kaynia, High-speed railway lines on soft ground: dynamic behaviour at critical train speed, *Journal of Sound and Vibration* 231 (3) (2000) 689–701. doi:10.1006/jsvi.1999.2647.
- [13] X. Sheng, C. Jones, D. Thompson, Prediction of ground vibration from trains using the wavenumber finite and boundary element methods, *Journal of Sound and Vibration* 293 (3-5) (2006) 575–586.
- [14] H. Chebli, D. Clouteau, L. Schmitt, Dynamic response of high-speed ballasted railway tracks: 3D periodic model and in situ measurements, *Soil Dynamics and Earthquake Engineering* 28 (2) (2008) 118–131. doi:10.1016/j.soildyn.2007.05.007.
- [15] G. Degrande, D. Clouteau, R. Othman, M. Arnst, H. Chebli, R. Klein, P. Chatterjee, B. Janssens, A numerical model for ground-borne vibrations from underground railway traffic based on a periodic finite element–

- boundary element formulation, *Journal of Sound and Vibration* 293 (3-5) (2006) 645–666.
- 465 [16] Z. Ozdemir, P. Coulier, M. Lak, S. François, G. Lombaert, G. Degrande, Numerical evaluation of the dynamic response of pipelines to vibrations induced by the operation of a pavement breaker, *Soil Dynamics and Earthquake Engineering* 44 (2013) 153–167.
- [17] D. Clouteau, R. Cottereau, G. Lombaert, Dynamics of structures coupled with elastic media – a review, *Journal of Sound and Vibration* 332 (10) 470 (2013) 2415–2436. doi:10.1016/j.jsv.2012.10.011.
- [18] B. R. Mace, D. Duhamel, M. J. Brennan, L. Hinke, Finite element prediction of wave motion in structural waveguides, *The Journal of the Acoustical Society of America* 117 (2005) 2835–2842. doi:10.1121/1.1887126.
- 475 [19] J.-M. Mencik, D. Duhamel, A wave-based model reduction technique for the description of the dynamic behavior of periodic structures involving arbitrary-shaped substructures and large-sized finite element models, *Finite Elements in Analysis and Design* 101 (2015) 1–14. doi:10.1016/j.finel.2015.03.003.
- 480 [20] Q. Serra, M. N. Ichchou, J.-F. Deü, Wave properties in poroelastic media using a Wave Finite Element Method, *Journal of Sound and Vibration* 335 (2015) 125–146. doi:10.1016/j.jsv.2014.09.022.
- [21] H. Pinault, E. Arlaud, E. Balmès, A general superelement generation strategy for piecewise periodic media, *Journal of Sound and Vibration* 485 469 (115133) (2020) 1–16. doi:10.1016/j.jsv.2019.115133.
- [22] L. Hall, Simulations and analyses of train-induced ground vibrations in finite element models, *Soil Dynamics and Earthquake Engineering* 23 (5) (2003) 403–413.

- [23] V. Alves-Fernandes, Numerical analysis of nonlinear soil behavior and heterogeneity effects on railway track response, Ph.D. thesis, Ecole Centrale Paris, Paris (2014).
490
- [24] N. M. F. Araújo, High-speed trains on ballasted railway track: dynamic stress field analysis, Ph.D. thesis, University of Minho, Braga (2010).
- [25] J. Bielak, P. Christiano, On the effective seismic input for non-linear soil-structure interaction systems, Bulletin of the Seismological Society of America 12 (1984) 107–119. doi:10.1002/eqe.4290120108.
495
- [26] J. W. Rayleigh, On waves propagated along the plane surface of an elastic solid, Proceedings of the London Mathematical Society s1-17 (1) (1885) 4–11. doi:10.1112/plms/s1-17.1.4.
- [27] L. Fryba, Elastic space with a moving force, in: Vibration of solids and structures under moving loads, Springer, 1972, pp. 269–284.
500
- [28] G. Eason, J. Fulton, I. N. Sneddon, The generation of waves in an infinite elastic solid by variable body forces, Philosophical Transactions of the Royal Society of London. Series A, Mathematical and Physical Sciences 248 (955) (1956) 575–607.
505
- [29] D. D. Ang, Transient motion of a line load on the surface of an elastic half-space, Quarterly of Applied Mathematics 18 (3) (1960) 251–256.
- [30] I. N. Sneddon, The stress produced by a pulse of pressure moving along the surface of a semi-infinite solid, Rendiconti del Circolo Matematico di Palermo 1 (1) (1952) 57–62.
510
- [31] J. Cole, J. Hugh, Stresses produced in a half-plane by moving loads, Journal of Applied Mechanics 25 (1958) 433–436.
- [32] L. Fryba, Force moving on elastic half-space, in: Vibration of solids and structures under moving loads, Springer, 1972, pp. 285–305.

- 515 [33] D. L. Lansing, The displacements in an elastic half-space due to a moving concentrated normal load, Tech. Rep. R238, NASA (1966).
- [34] G. Eason, The stresses produced in a semi-infinite solid by a moving surface force, *International Journal of Engineering Science* 2 (6) (1965) 581–609.
- [35] M. Papadopoulos, The use of singular integrals in wave propagation problems; with application to the point source in a semi-infinite elastic medium, *Proceedings of the Royal Society of London. Series A. Mathematical and Physical Sciences* 276 (1365) (1963) 204–237.
- 520 [36] R. Payton, An application of the dynamic betti-rayleigh reciprocal theorem to moving-point loads in elastic media, *Quarterly of Applied Mathematics* 21 (4) (1964) 299–313.
- 525 [37] J. Mandel, A. Avramesco, Déplacements produits par une charge mobile à la surface d’un semi-espace élastique [Displacements generated by a moving load on the surface of an elastic semi-space], *Comptes rendus hebdomadaires des séances de l’Académie des Sciences* 252 (24) (1961) 3730–+.
- 530 [38] R. D. Woods, Screening of surface waves in soils, *Journal of the Soil Mechanics and Foundations Division: proceedings of the American Society of Civil Engineers* 94 (4) (1968) 951–979.
- [39] V. Krylov, Stochastically rough surfaces as seismic barriers against railway-induced ground vibrations, in: *Ground Vibrations from High-Speed Railways: Prediction and mitigation*, ICE Publishing, 2019, pp. 337–358.
- 535 [40] F. Gustafsson, Determining the initial states in forward-backward filtering, *IEEE Transactions on Signal Processing* 44 (1996) 988–992. doi:10.1109/78.492552.
- [41] T. Hoang, D. Duhamel, G. Forêt, H. P. Yin, P. Joyez, R. Caby, Calculation of force distribution for a periodically supported beam subjected to moving loads, *Journal of Sound and Vibration* 388 (2017) 327–338.
- 540

- [42] D. Komatitsch, J. Tromp, Introduction to the spectral element method for three-dimensional seismic wave propagation, *Geophysical journal international* 139 (3) (1999) 806–822.
- 545 [43] L. de Abreu Corrêa, J. C. Quezada, R. Cottureau, S. Costa d’Aguiar, C. Voivret, Randomly-fluctuating heterogeneous continuum model of a granular medium, *Computational Mechanics* 60 (5) (2017) 845–861. doi:10.1007/s00466-017-1446-8.
- [44] G. Gatti, S. Touhami, F. Lopez-Caballero, R. Paolucci, D. Clouteau, 550 V. Alves Fernandes, M. Kham, F. Voldoire, Broad-band 3-D earthquake simulation at nuclear site by an all-embracing source-to-structure approach, *Soil Dynamics and Earthquake Engineering* 115 (2018) 263–280. doi:10.1016/j.soildyn.2018.08.028.
- [45] F. Gatti, F. Lopez-Caballero, D. Clouteau, R. Paolucci, On the effects of 555 the 3-D regional geology on the seismic design of critical structures: the case of the Kashiwazaki-Kariwa nuclear power plant, *Geophysical Journal International* 213 (2) (2018) 1073–1092. doi:10.1093/gji/ggy027.
- [46] F. Gatti, D. Clouteau, Towards blending physics-based numerical simulations and seismic databases using Generative Adversarial Network, 560 *Computational Methods in Applied Mechanics and Engineering* 372 (113421) (2020) 1–27. doi:10.1016/j.cma.2020.113421.
- [47] L. de Abreu Corrêa, R. Cottureau, B. Faure, Dispersion analysis in ballasted railway tracks and anderson localization in granular media, *Journal of Sound and Vibration* 465 (115010) (2019) 1–13. doi:10.1016/j.jsv.2019.115010. 565